Powder Technology 342 (2019) 371–379

Contents lists available at ScienceDirect

Powder Technology

journal homepage: www.elsevier.com/locate/powtec

Selective laser melting of titanium parts: Influence of laser process parameters on macro- and microstructures and tensile property

Dongsheng Sun [a,b], Dongdong Gu [a,b,*], Kaijie Lin [a,b], Ji Ma [a,b], Wenhua Chen [a,b], Jie Huang [c], Xiaofeng Sun [c], Mingqiang Chu [c]

[a] College of Materials Science and Technology, Nanjing University of Aeronautics and Astronautics, Yudao Street 29, Nanjing 210016, Jiangsu Province, PR China
[b] Jiangsu Provincial Engineering Laboratory for Laser Additive Manufacturing of High-Performance Metallic Components, Nanjing University of Aeronautics and Astronautics, Yudao Street 29, Nanjing 210016, Jiangsu Province, PR China
[c] Aeronautical Manufacturing Technology Institute, Shanghai Aircraft Manufacturing Co., Ltd, Shanghai 201324, PR China

ARTICLE INFO

Article history:
Received 10 March 2018
Received in revised form 2 September 2018
Accepted 26 September 2018
Available online 27 September 2018

Keywords:
Selective laser melting
Titanium alloys
Parameter optimization
Dimensional accuracy
Tensile property

ABSTRACT

The laser process parameters play an important role in the macro- and microstructures and tensile property of titanium samples fabricated by selective laser melting (SLM). In this study, the effect of laser process parameters on the density, surface morphology, dimensional accuracy, microstructure and tensile property of SLMed Ti6Al4V parts was investigated. With the increase of laser power and decrease of scan speed, the densification increased and the relative density showed reduced sensitivity to laser power under higher laser power (>175 W). The morphology of scan tracks on the top surface changed from clear and uniform mode to disordered mode with the increase of scan speed. The marks of melt flow, molten pool overlap and adhered powder could be observed obviously on the side surface. In the analysis of dimensional accuracy, the size shrinkage effect in the building direction (z-axis) was discussed and the "periphery spreading effect" in horizontal direction (x-axis and y-axis) was presented. Martensite α' was the main constituent phase in SLMed Ti6Al4V samples. With the increase of scan speed, the width of prior β grains decreased gradually and the formed α' phase changed into a relatively refined acicular shape. Conclusively, the relationship between microstructure and tensile property was discussed and a relative high tensile property was obtained.

1. Introduction

SLM technology is a promising technology to fabricate novel components and structures with complex geometries [1–3]. For mass production-scale, SLM has an obvious advantage to compress the industry chain and to reduce the waste of materials, especially as compared to conventional materials removal methods [4]. SLM technology can be used to fabricate three-dimensional fully functional parts from metal powder by fusing the material in a layer by layer manner [5–7]. To date, most of the SLM researches revolved around four types of metals: titanium, iron, aluminum and nickel. These metals were selected due to their widespread application and their advantages for SLM [8]. In the last decade, the number of publications of SLM of titanium were second to that of steel; especially Ti6Al4V had become the most commonly researched metals due to their wide range of applications as well as the relatively high performances obtained from the SLM process [9].

As SLM is a layer-by-layer build technology, it provides numerous opportunities to tailor the microstructure and subsequently the anticipated mechanical properties. However, the quality of SLM produced parts is highly dependent on parameters applied in this process [10]. So, there is a need to optimize the process parameters from technological view. By optimizing the process parameters, a correct adjustment of parameters can be obtained and the quality of the SLMed parts can be improved. Many researchers have conducted studies on the relationship among process parameters, quality, microstructure and property of SLMed parts. The development of the microstructure of the Ti6Al4V alloy processed by SLM and the influence of the scanning parameters and scanning strategy on this microstructure were studied by Thijs et al. [11]. Song et al. [12] confirmed that process parameters played a significant role in microstructure, roughness, densification and microhardness of SLMed Ti6Al4V parts. Sun et al. [13] found that powder thickness was the most significant influence in process parameters on the density SLMed Ti6Al4V. Sample with density higher than 95% was obtained and the microstructure of sample was mainly composed of α' acicular martensite, α phase and β phase. The surface structure and porosity of Ti6Al4V samples fabricated by SLM under different laser scan speeds and powder layer thicknesses had been studied by Qiu

* Corresponding author at: College of Materials Science and Technology, Nanjing University of Aeronautics and Astronautics, Yudao Street 29, Nanjing 210016, Jiangsu Province, PR China.
E-mail address: dongdonggu@nuaa.edu.cn (D. Gu).

https://doi.org/10.1016/j.powtec.2018.09.090
0032-5910/

et al. [14]. It was found that at a high laser power and a fixed powder layer thickness (20 μm), the samples contained particularly low porosity when the laser scan speeds were below 2700 mm/s. Shi et al. [15] found that the high layer thickness played a key role on surface roughness rather than tensile properties during the SLM process. The Ti6Al4V tensile samples were fabricated by SLM under high layer thickness. Although a sample with a relatively coarse surface was generated, the average values of yield strength, ultimate tensile strength, and elongation were 1050 MPa, 1140 MPa, and 7.03%, respectively. The influence of three process parameters (i.e. laser power, scan speed and hatch distance) on the relative density was studied by Li et al. [16]. Compared with laser power, scan speed and hatch distance by taguchi method, it was found that the scan speed had the greatest effect on the relative density. Han et al. [17] investigated the relative densities and microhardness in the optimized processing window. The alternation regularity between the laser energy per unit volume and microstructure was researched. The SLMed Ti6Al4V sample with a tensile strength of 1268 MPa, a yield strength of 1030 MPa, and an elongation of 4.2% could be obtained by using the optimized range of the laser energy per unit volume. Besides working on SLMed Ti6Al4V, Calignano et al. [18] investigated the effect of three important SLM process parameters, namely scan speed, laser power and hatching distance, on the surface roughness of direct metal laser sintering (DMLS) processed aluminum specimens. They found that the scan speed had the greatest influence on the surface roughness of aluminum samples produced by DMLS compared to other parameters such as laser power and hatching distance. Abd-Elghany and Bourell [19] evaluated the part geometry, dimensional tolerance, surface quality, density, mechanical properties and microstructure of SLMed 304 L stainless steel under different layer thicknesses and laser scan speeds. The results revealed that using small layer thickness and low scan speed improved the tensile properties by >20%. From the above literature review, in order to enhance the quality and performance of SLMed Ti6Al4V parts, the relationship among process parameters, macro- and microstructures should be further investigated. Among the process parameters, one of the most important is the laser scan speed, because it directly affects the laser energy density in the powder bed and the process time [20].

The macrostructures and microstructures were the macro and micro characteristics of SLMed metal parts, respectively. Controlling macrostructures and microstructures of SLMed metal component is the key for the quality control of SLM. The objective of the present work is to investigate the influence of laser process parameters on the macrostructures (densification behavior, dimensional accuracy) and microstructures (surface morphology of molten pool and scan tracks). The samples with the best quality were obtained by optimizing the process parameters. Martensite α' was the main constituent phase in as-fabricated Ti6Al4V samples. The as-fabricated samples exhibited high tensile strengths (a tensile strength of 1103.16 MPa) but poor ductilities with elongation generally smaller than 5%.

2. Experimental procedures

2.1. Powder characteristics

In this study, the gas atomized Ti6Al4V powder with the size range of 15–53 μm (D10: 23.23 μm, D50: 35.91 μm, D90: 50.11 μm) supplied by TLS Technik GmbH was used. The powder has a spherical shape and the morphology of powder is shown in Fig. 1 (a).

2.2. SLM process

The SLM 150 machine mainly consisted of an IPG Photonics Ytterbium YLR-500-SM fiber laser (IPG, Germany) with a maximal laser power of 500 W and a focused laser spot diameter approaching 70 μm, an automatic powder paving apparatus, an inert argon gas protection system and a computer system for process controlling. Some cubic samples with the dimensions of 10 mm × 10 mm × 5 mm and tensile specimens were fabricated on the pure Ti substrate plate. The SLM process was conducted under argon atmosphere and the O_2 content was maintained below 100 ppm. The SLM parameters of cubic samples were listed as follow: laser power $P = 100$ W – 250 W, scan speed $v = 600$ mm/s – 1200 mm/s, hatch space $h = 50$ μm and powder layer thickness $t = 50$ μm. The scanning strategy for the successive layers was inter-layer stagger and then orthogonal scanning strategy (Fig. 1(b)) [21–23]. In order to fabricate the mechanical properties test samples in optimum condition, the experiment was conducted using the optimized parameter of the density test. A laser power of 225 W, scan speed of 600 mm/s, 1000 mm/s, 1200 mm/s, hatching distance of 50 μm and powder layer thickness of 50 μm were used to fabricate the standard tensile plates with dog bone shape.

2.3. Surface morphology

A scanning electron microscope (SEM) was applied to obtain the top and side surface morphologies of SLMed Ti6Al4V samples.

2.4. Dimensional accuracy

SLM is a kind of manufacturing technology with the high forming accuracy compared to traditional processing methods [24–26]. There are a lot of factors that can influence the dimensional accuracy, including melting of metal powder, spatter of molten drop and flow of molten pool. In fact, the dimensional error can be used as a visual and convenient model to evaluate the dimensional accuracy of SLMed parts. The dimensional errors in horizontal direction (x-axis and y-axis) and building direction (z-axis) were measured, respectively. The dimensional error was calculated using:

$$de = (x_m\text{-}x_d)/x_d \quad (1)$$

where the x_m was the measured value and x_d was the designing value.

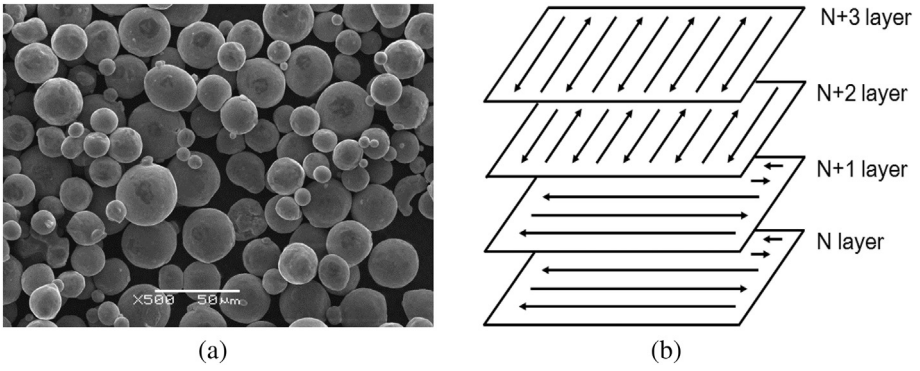

Fig. 1. (a) FE-SEM images displaying the typical morphologies of the as-used Ti6Al4V powder; (b) the schematic presentation of laser scanning strategy.

2.5. Microstructural evolution

For microstructural observation, the SLMed Ti6Al4V samples were first ground using the SiC grinding paper up to 5000 grit size and polished using SiO_2 slurry. The polished surfaces were etched by Korll reagent (H_2O: HNO_3: HF = 1 mL: 3 mL: 50 mL). An optical microscope (OM) was used to observe the interlayer macrostructure and microstructure characterization on cross-sections of cubic parts.

Phase identification was conducted by X-ray diffraction (XRD) using a D8 Advance x-ray diffractometer (Bruker AXS GmbH, Germany), using a continuous scan mode. A scan at 5°/min was conducted over a wide range of 20–90° and a general overview of the diffraction peaks was obtained.

2.6. Tensile properties tests

Ultimate Tensile Strength and Elongation (%) of SLMed Ti6Al4V samples were achieved from the tensile tests according to GB/T 228.1-2010 standard. A tensile testing machine (MTS E45.105) with 0.2 mm/s test speed was used. Subsequently, the tensile fracture morphology was observed by SEM.

3. Results and discussion

3.1. Densification behavior

Densification behavior is one of the most important aspects during SLM process which needs to be analyzed in depth, because it has a significant influence on the performance of the SLMed components. The densification behavior is affected by many process parameters, while this work is focused only on the effect of laser power *P* and scan speed *v*. The relative densities of all samples were measured and depicted in Fig. 2. As a whole, with the increase of laser power and the decrease of scan speed, the relative density of SLMed Ti6Al4V parts grew. The high density of SLMed Ti6Al4V parts could be obtained under high laser power and low scan speed, which could be up to 99%. Furthermore, when the laser power was set as 175 W, the relative density of SLMed parts grew rapidly with the increase of laser power, however, the relative density increased slowly over 175 W. The relative density showed reduced sensitivity to laser power under higher laser power. In the region of low laser power (<150 W), the energy density during SLM process was not large enough to melt Ti6Al4V powder, the width of the molten pool was small, which resulted in an insufficient overlap between the scan tracks. The insufficient overlap was a cause of formation of the unmelted powder between the scan tracks. In the melting process of a new layer, it became difficult to fully remelt these powder.

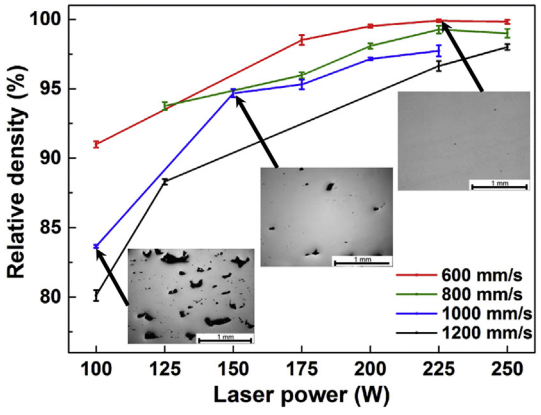

Fig. 2. Relative densities of the SLMed Ti6Al4V parts with different process parameters corresponding to macrostructure images.

As a consequence, incomplete fusion holes were formed and remained in the SLM fabricated part.

The layerwise macrostructures on cross-sections of SLMed Ti6Al4V parts fabricated under different scan speeds were observed (Fig. 3). When laser power *P* was 225 W, with the increase of scan speed, the density of SLMed Ti6Al4V part decreased sharply owing to the dramatic increase of interlayer pores. When scan speed was lower, the temperature of molten pool was generally high due to the intense laser energy density. In this case, the complete fusion of the Ti6Al4V powder was observed and the melt spreaded completely. At a relatively high scan speed, the energy input was too low to fully melt the powder and the molten pool underwent a significant disturbance and even interruption, generating a discontinuous molten pool. Consequently, it was difficult to fill completely the pores between layer and layer, hence causing interlayer pores and a limited densification response (Fig. 3(d)). In addition, the presence of discontinuity scan tracks and cave-like pores on the top surface improved the surface roughness. Then, the increased surface roughness could cause inhomogeneous powder spreading and distribution of the subsequent layers, causing the inconsistent melt flow and melt pool, and thus high porosity.

3.2. Surface morphology

Surface morphology is a significant microstructure characteristic that can evaluate the quality of SLMed parts. The top surface morphologies of the SLMed Ti6Al4V are shown in Fig. 4. When the laser power *P* was 225 W and scan speed *v* was 600 mm/s, a clear and uniform liquid solidification front without balling phenomenon was observed on the top surface (Fig.4(a)). When the laser power was kept constant ($P = 225$ W) and the scan speed increased to 800 mm/s, although the scan tracks became irregular, it was still visible as shown in Fig. 4(b). At 1000 mm/s, the incomplete spreading on the top surface was observed (Fig. 4(c)). When the scan speed further increased to 1200 mm/s, the liquid solidification front became considerably disordered. Interrupted scan tracks and small size balls ("balling" effect) were observed on the top surface. Besides, more pores were appeared on the top surface and some unmelted powder could be observed in pores (Fig. 4(d)).

Fig. 5 illustrates the typical side surface morphologies of the SLMed Ti6Al4V parts fabricated at 600 mm/s and 1200 mm/s. When the laser power *P* was 225 W, the side surface of SLMed Ti6Al4V part at a low scan speed of 600 mm/s was completely dense. Continuous scan tracks and regular overlap of molten pool were observed obviously (Fig. 5(a)), although a number of unmelted powder attached on the side surface. When scan speed reached 1200 mm/s, some interlayer pores and a large amount of balls were observed at the surface (Fig. 5(b)). The overlap of molten pool could not be observed and the marks of melted flow changed from regular mode to disorderly mode. The presence of a large of balls and disorderly marks of melt flow resulted in a poor surface quality.

From the above observation, the SLM parameter of scan speed significantly affected the top and side surface morphology of the SLMed Ti6Al4V samples. Fundamentally, a higher scan speed led to a shorter dwelling time of laser beam and attendant a lower temperature in the molten pool. The relationship between dynamic viscosity μ and temperature *T* could be evaluated by Iida and Guthrie [27]:

$$\mu = (16/15)\sqrt{m/KT}\sigma \tag{2}$$

where *m* is the atomic mass, σ is the surface tension of Ti6Al4V liquid and *T* is the temperature of molten pool, a lower molten pool temperature resulted in a higher viscosity. Based on Eötvös 's results [28], the surface tension σ could be calculated by means of the following equation:

$$\sigma = K(T_c - T)(M/\rho)^{\frac{2}{3}} \tag{3}$$

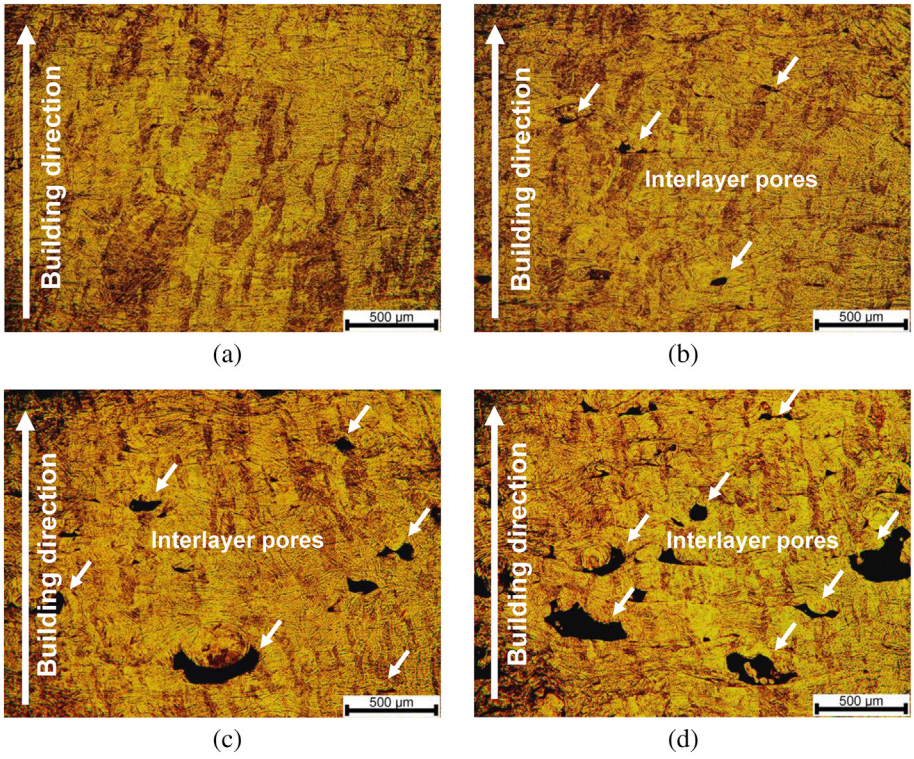

Fig. 3. OM images showing interlayer macrostructures on cross-sections of SLMed Ti6Al4V parts under different scan speed ($P = 225$ W): (a) 600 mm/s; (b) 800 mm/s; (c) 1000 mm/s; (d) 1200 mm/s.

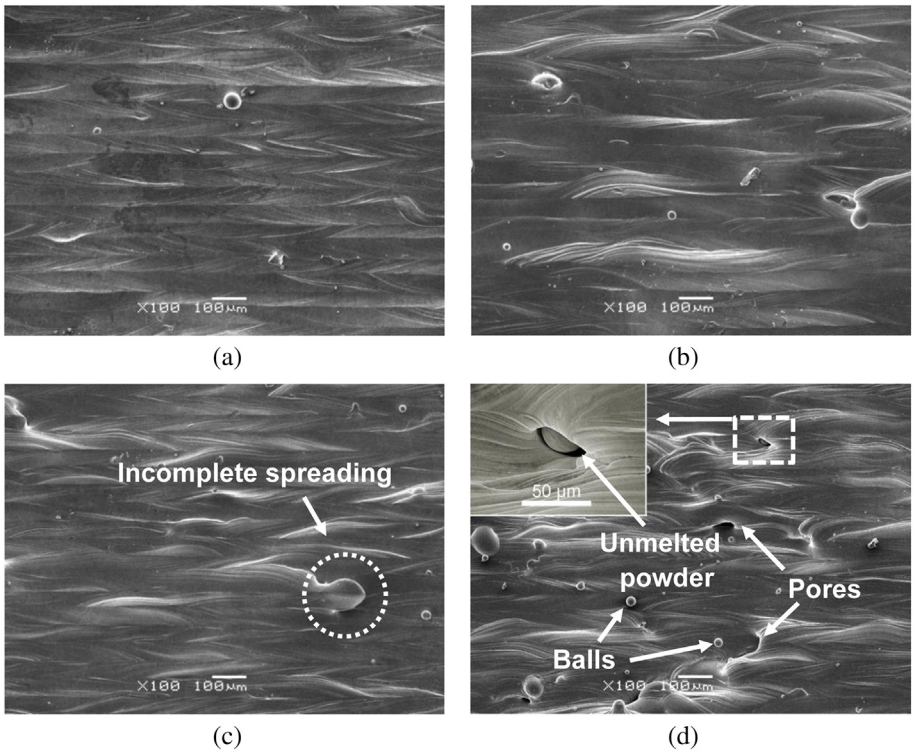

Fig. 4. Top surface morphologies of SLMed Ti6Al4V parts under different scan speed ($P = 225$ W): (a) 600 mm/s; (b) 800 mm/s; (c) 1000 mm/s and (d) 1200 mm/s.

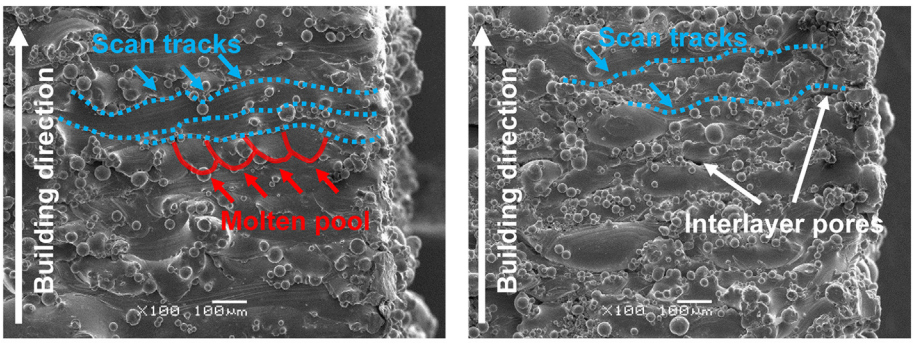

(a) (b)

Fig. 5. Side surface morphology of SLMed Ti6Al4V parts fabricated at various scan speeds ($P = 225$ W): (a) 600 mm/s and (b) 1200 mm/s.

where M is the molecular weight of liquid, ρ is the density of Ti6Al4V liquid, T_c is the critical temperature and T is the molten pool temperature. The surface tension increased with the reducing of molten pool temperature. Actually, the high viscosity and surface tension of molten pool resulted from the higher scan speed could lead to an unstable flow on the top surface (Fig. 4(b) (c) (d)) and more adhesion of powder on the side surface (Fig. 5(b)).

Besides that, higher scan speed also led to a larger temperature gradient in the molten pool, and consequently a more intense Marangoni convection and liquid capillary instability were presented in the molten pool [29].

3.3. Dimensional accuracy

Dimensional accuracy is an important macro characteristic of SLMed parts. As shown in Fig. 6(a) and (b), the dimensional error in horizontal direction (x-axis and y-axis) rose rapidly with the increase of laser power. A lower scan speed also led to a higher dimensional error in horizontal direction (x-axis and y-axis). The variation of the dimensional errors in horizontal direction (x-axis and y-axis) induced by change of scan speed was larger at low scan speed, however, the data of dimensional errors in horizontal direction (x-axis and y-axis) showed a concentrated distribution when scan speed was comparatively high. The degree of melting got higher as the laser power increased in building direction (z-axis direction), resulting in a stronger shrinkage effect and a final large dimensional error (Fig. 6(c)). At low scan speed of 600 mm/s and 800 mm/s, with the increasing of laser power, concentration of dimensional error in z-axis direction got stable which showed the Ti6Al4V powder had been fully melted and spreaded.

The key to forming quality assurance is the fusion of metal powder during SLM process [30,31]. In rapid prototyping technology, the metal powder is heated, melted and subsequent spreading under the radiation of laser beam. These processes play a significant role in the dimensional errors of SLMed Ti6Al4V cubic samples in horizontal direction and building direction.

In horizontal direction (x-axis or y-axis), the positive value of the dimensional error was measured. The edge of as-built Ti6Al4V part was observed when the laser power P was 225 W and the scan speed v was 600 mm/s as shown in Fig. 7(a). The "periphery spreading effect" caused by melt spreading occurred on the edges of the SLMed Ti6Al4V samples (Fig. 7(b)). As shown in Fig. 7(a), the continuous scan tracks and molten pool located at the edge of SLMed Ti6Al4V part were observed clearly. Near the edge of the samples, as a result of the existence of gravity, Fig. 7(a) presented obviously the tendency that the melt flow from inside to outside, which corresponded to the "periphery spreading effect" (Fig. 7(b)). According to the discussion all above, the low surface tension σ and dynamic viscosity μ played a positive role in melt flow and the attendant high dimensional accuracy in horizontal direction (x-axis or y-axis). With a relatively low scan speed, the higher energy density led to a lower surface tension σ and dynamic viscosity μ, leading to the liquidity of melt increasing in horizontal direction

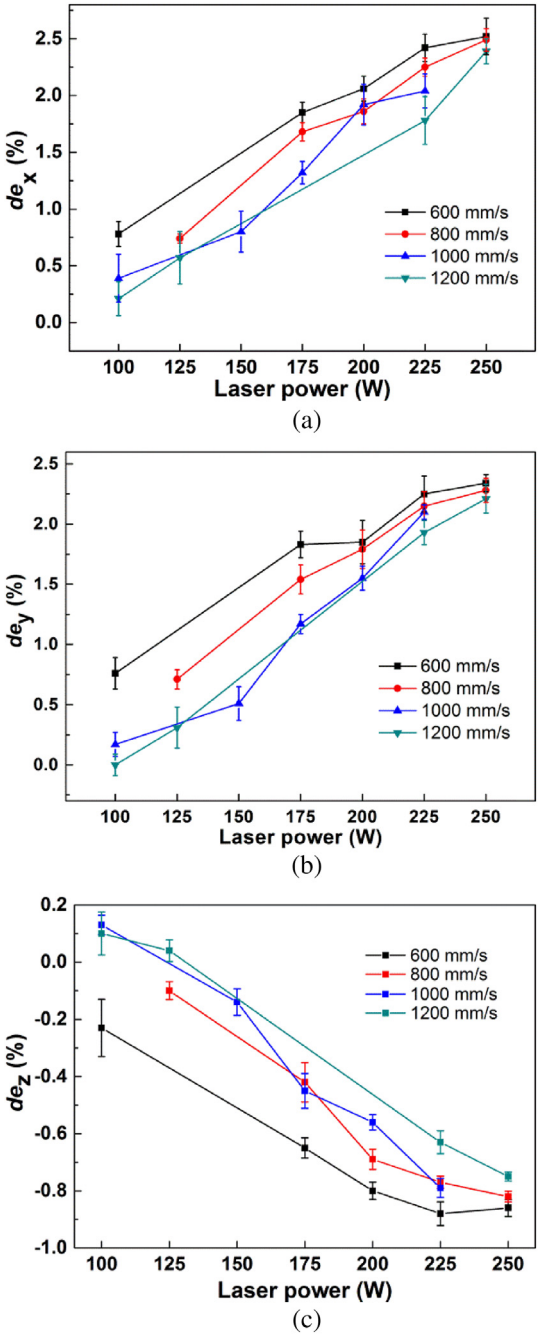

Fig. 6. Dimensional errors in different direction at various process parameters (P, v): (a) in x-axis direction; (b) in y-axis direction and (c) in z-axis direction.

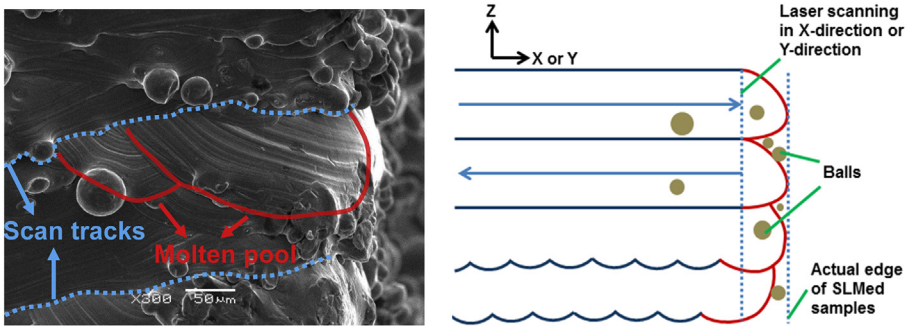

Fig. 7. (a) Side surface morphology of SLMed Ti6Al4V parts fabricated at $v = 600$ mm/s and $P = 225$ W and (b) the schematic showing the powder adhesion phenomenon and the "spreading effect" of the edge of SLMed part.

(x-axis or y-axis). The "periphery spreading effect" became more significant when the scan speed was high. In addition, the powder adhesion and the "balls" phenomenon could increase the dimensional error in horizontal direction (x-axis and y-axis).

The gap between powder particles would be filled under the laser irradiation, resulting in the shrinkage in building direction (z-axis). The actual forming thickness of each layer was less than that of the powder laying. The relatively worse accuracy building direction could be ascribed to the shrinkage of the each powder layer [32]. The shrinkage rate d $(\Delta L/L0)$/ dt during SLM solidification could be evaluated by Zhu et al. [33]:

$$\mathrm{d}(\Delta L/L_0)/\mathrm{d}t = \Delta PW/2R\mu \quad (4)$$

where ΔP is the capillary pressure, R the grain radius, W the liquid thickness and μ is the viscosity of the liquid. Combining Eq. (2) with Eq. (4), when using a lower scan speed and a higher laser power, the lower dynamic viscosity of Ti6Al4V liquid was obtained, resulting in the higher dimensional error in building direction (z-axis). As the scan speed increased to higher values, the unstable melt flow, higher dynamic viscosity and surface tension led to higher surface roughness which could compensate the shrinkage effect in building direction (z-axis). In addition, the balling phenomenon and the incomplete spreading on the samples surface had some effects on the compensation for the shrinkage effect in building direction (Fig. 4(d)). The extremely rapid melting/ cooling stages during the Ti6Al4V SLM process offered a transformation of martensite which could influence the dimensional error in building direction (z-axis) [34].

3.4. Microstructural evolution

The characteristic crystalline structures of SLMed Ti6Al4V parts developed under various scan speed conditions are shown in Fig. 8. Elongated grains were observed growing through the SLM layers (50 μm). Furthermore, martensite plates were visible within the elongated grains, as reported in the previous studies [11,35–38]. Obviously, when laser power was kept constant ($P = 225$ W), a relatively low scan speed and attendant high energy input resulted in coarse prior β grains. A lot of martensite plates formed in the inner part of these coarse prior β grains. With the increase of scan speed, the width of

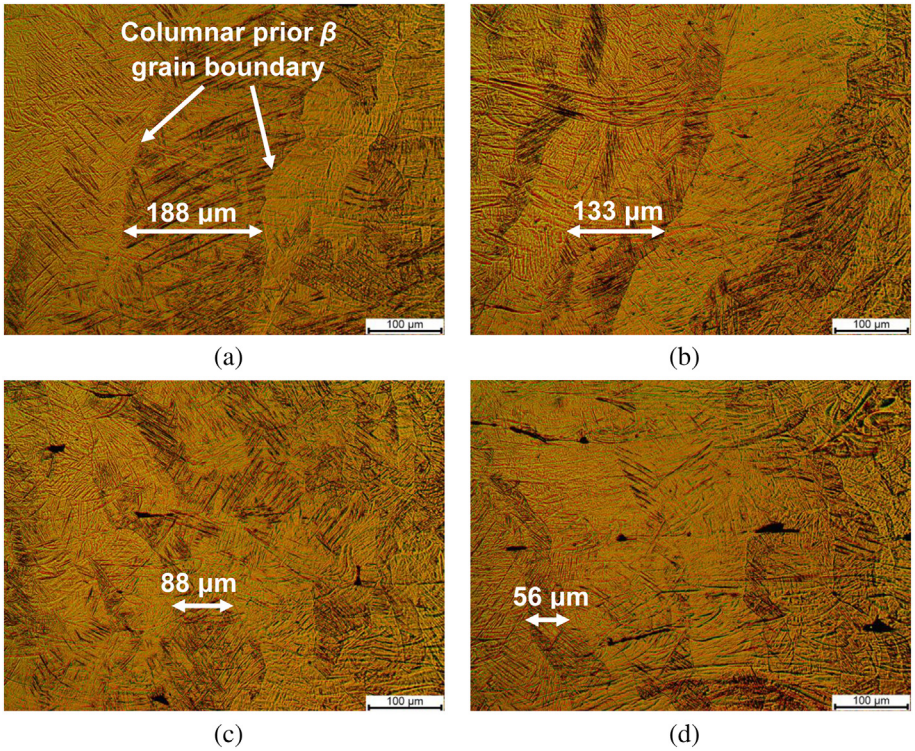

Fig. 8. Cross-sectional microstructure of SLMed Ti6Al4V parts fabricated at different scan speeds ($P = 225$ W): (a) 600 mm/s; (b) 800 mm/s; (c) 1000 mm/s and (d) 1200 mm/s.

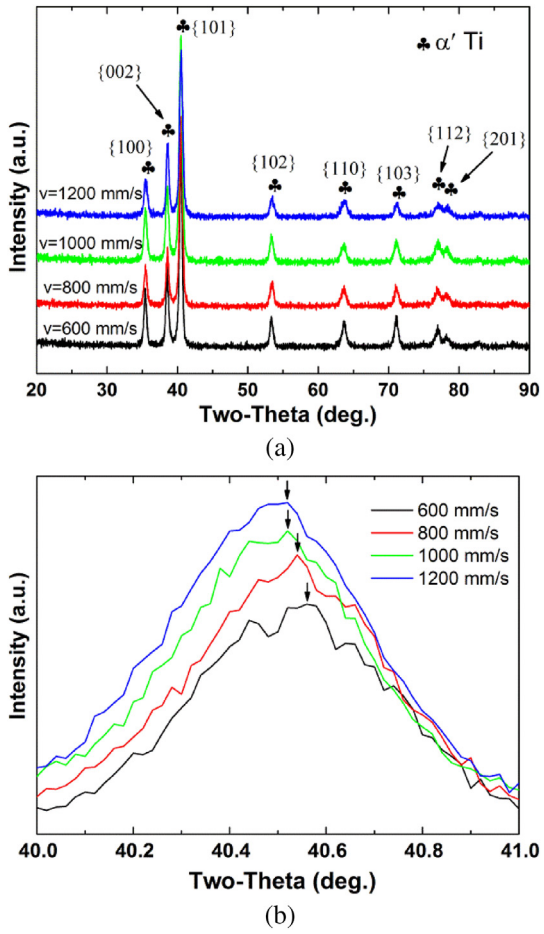

Fig. 9. XRD spectrum of SLMed Ti6Al4V parts using different process parameters obtained over a wide range of $2\theta = 20–90°$ (a) and in a small range of $2\theta = 40–41°$.

prior β grains decreased gradually and the formed α' phase changed into a relatively refined acicular shape.

Fig. 9(a) shows the XRD spectrum of SLMed Ti6Al4V at different scan speeds ($P = 225$ W). The XRD spectrum exhibited the characteristic of the hexagonal close-packed (hcp) structure of Ti including α and α'. Here, the standard diffraction peaks for hcp Ti (α phase), located at $2\theta = 38.455°$ and $2\theta = 40.251°$, were taken for a comparison. The 2θ locations of the diffraction peaks of all Ti6Al4V samples fabricated by SLM for hcp Ti generally shifted to higher 2θ. These hcp Ti diffraction peaks corresponded to martensitic α' phase. There were no obvious peaks of β phase found in these samples. So martensite α' was the main constituent phase of SLMed Ti6Al4V samples. Fig. 9(b) shows the details of XRD spectrums of SLMed Ti6Al4V at different scan speeds. The peaks slightly shifted towards low diffraction angles with increasing scan speed. As we all know, Al and V act as substitutional solutes in α'-Ti matrix, and their radii (0.143 nm for Al and 0.132 nm for V) are smaller than that of Ti (0.147 nm) [39]. A low scan speed of 600 mm/s could lead to a longer dwelling time of the laser beam on the surface of melt pool, thereby giving excessive energy to the pool and elevating temperature of molten pool significantly. The higher solid solubility of Al and V could be obtained in the α'-Ti matrix. Therefore, the lattice parameters of α'-Ti became smaller and the corresponding diffraction peaks shifted to higher angles with the decrease of scan speed.

3.5. Tensile properties and fracture mechanisms

The stress-strain curves of SLMed Ti6Al4V plate samples fabricated at various scan speeds of 600 mm/s, 1000 mm/s and 1200 mm/s ($P = 225$ W) are shown in Fig. 10. It could be seen that the SLMed Ti6Al4V samples generally showed high ultimate tensile strength (UTS), which were found to be obviously superior to that of the standard materials from the ASM Materials Properties Handbook [40]. However, the SLMed Ti6Al4V samples exhibited fairly low elongations, which were well below that of wrought Ti6Al4V alloy (about 10%) due to the existence of inner defects and non-equilibrium martensitic phase α'. Remarkably, an optimal process parameter of SLMed Ti6Al4V ($P = 225$ W, $v = 600$ mm/s) was achieved, corresponding the highest tensile strength (1103.16 MPa) and elongation to break (4.09%).

To better understand the tensile fracture mechanism and the fracture regulation of SLMed Ti6Al4V samples fabricated at various scan speeds, an investigation on the tensile fracture surfaces has been carried out. The representative tensile fracture surfaces of SLMed Ti6Al4V samples are shown in Fig. 11. As shown in Fig. 11(a), the fracture surfaces of the SLMed Ti6Al4V sample with the scan speed of 600 mm/s exhibited a mixed mode of the brittle and ductile fracture, showing predominant dimple network and cleavage plane. Cleavage fracture is a low energy brittle fracture which propagates along low index crystallographic planes [41]. The number and shape of the dimples on the tensile fracture surface indicated the extent of plastic deformation. Even though some dimple networks existed on the fracture surface of SLMed Ti6Al4V samples in the present work, the number and intensity of dimples was very low, in addition, the heterogeneous distribution of dimples was observed. The characteristic of surface fracture was well consistent with the tensile testing results.

An obvious difference can be observed in the fracture surface appearance of the SLMed Ti6Al4V samples with different scan speeds ($P = 225$ W). By contrast, at the scan speed of 1000 mm/s, the fracture surface of SLMed Ti6Al4V sample was characterized by uncombined regions and some dimple networks. These dimples presented more irregular shape compared with Fig. 11(a). The formation of uncombined regions were due to the selected inappropriate process parameters. A microcrack was observed in the uncombined region of fracture surface (Fig. 11(b)). As shown in Fig. 11(c), the most striking characteristic of the fracture surface was the presence of a number of unmelted powder. At a high scan speed of 1200 mm/s, the low laser energy density cannot be enough to melt the powder completely. The unmelted powder and uncombined region reduced the tensile property significantly. With the exception of these regions, the fracture surface of binding region was characterized by high-density dimple network. With the increase of scan speed, the width of prior β gradually decreases. The fine prior β was benefit to the ductility of SLMed Ti6Al4V parts, thus the high-density dimple networks with regular shape were observed. In general, the fracture of SLMed Ti6Al4V parts showed a mixed mode of brittle and ductile fracture. High tensile strength (1103.16 MPa) and comparably low elongation (4.09%) were obtained.

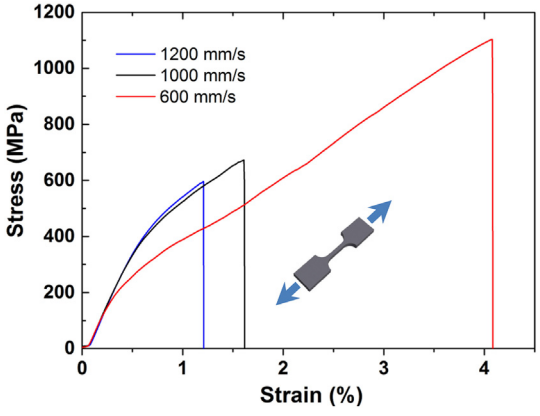

Fig. 10. Stress-Strain curves for SLMed Ti6Al4V samples fabricated at different scan speed ($P = 225$ W): 600 mm/s; 1000 mm/s and 1200 mm/s.

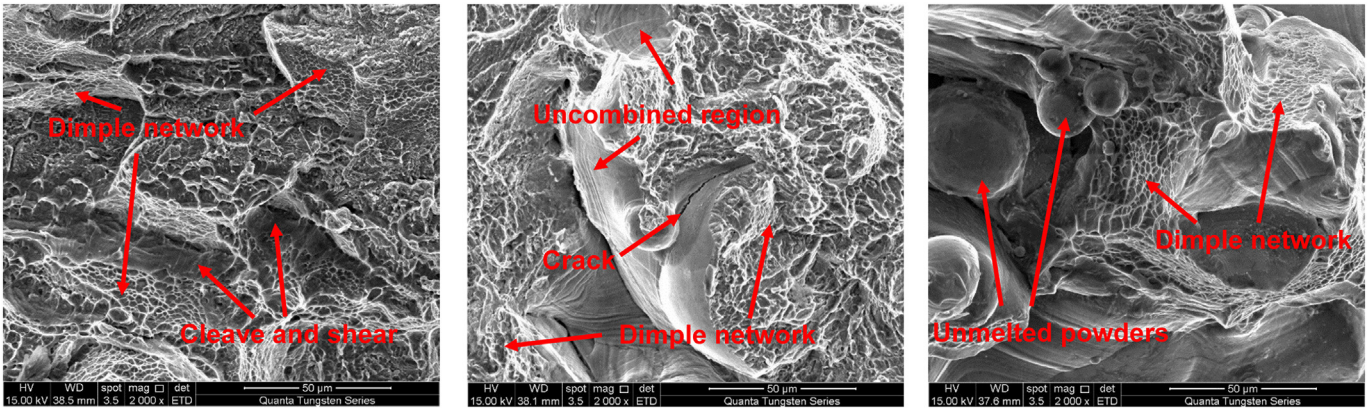

Fig. 11. Tensile fracture surfaces of SLMed Ti6Al4V samples fabricated at various scan speed ($P = 225$ W): (a) 600 mm/s; (b) 1000 mm/s and (c) 1200 mm/s.

4. Conclusions

The SLM manufacturing of Ti6Al4V samples has been carried out with a double objective: (1) determining the relationship among process parameter, macro- and microstructures, (2) investigating the tensile behavior and failure mechanisms on as-built samples.

After analysis of the macro- and microstructures of SLMed Ti6Al4V parts, it can be determined that with the increase of laser power and decrease of scan speed, the density increased and showed reduced sensitivity to laser power under higher laser power (>175 W). The scan tracks on the top surface morphology changed from clear and uniform mode to disordered mode with the increase of scan speed. In addition, a higher scan speed led to the "balls" phenomenon. On the side surface morphology, the melt flow, overlap of molten pool and balls could be observed obviously. In the analysis of dimensional accuracy, the size shrinkage in the building direction (z-axis) was discussed and the "periphery spreading effect" in horizontal direction (x-axis and y-axis) was presented on the base on melt flow. XRD showed the martensite α' was the main constituent phase in SLMed Ti6Al4V samples. With the increase of scan speed, the width of prior β grains decreased gradually and the formed α' phase changed into a relatively refined acicular shape.

The last part was focused on laser scan speed to deliver the best tensile property. The tensile property of as-built samples became worse with the increase of scan speed. When the laser power was 225 W and the scan speed was 600 mm/s, a high tensile strength (1103.16 MPa) and a comparably low elongation (4.09%) were obtained. The fracture surfaces SLMed Ti6Al4V samples exhibited a mixed mode of brittle and ductile fracture.

Dongsheng Sun is currently pursuing for a master's degree in College of Materials Science and Technology, Nanjing University of Aeronautics and Astronautics (NUAA), PR China. He received the bachelor degree in Material Formation and Control Engineering from Shandong Jianzhu University in Jun. 2016. His principal research interest selective laser melting (SLM), especially majoring in the experiments of titanium processed by SLM.

Professor Dongdong Gu is currently a Full Professor in College of Materials Science and Technology, Nanjing University of Aeronautics and Astronautics (NUAA), PR China. He received the Ph.D. in Materials Processing Engineering from NUAA in Jun. 2007. From Sep. 2009 to Aug. 2011, he worked in Fraunhofer Institute for Laser Technology ILT as the Alexander von Humboldt Research Fellow. His principal research interest is laser-based additive manufacturing including selective laser melting (SLM), direct metal laser sintering (DMLS), and laser metal deposition (LMD). Prof. Gu has authored/co-authored >120 papers in a number of internationally recognized peer-reviewed journals.

Dr. Kaijie Lin is currently a lecturer in College of Materials Science and Technology, Nanjing University of Aeronautics and Astronautics (NUAA), PR China. He received the Ph. D. in Materials Science and Engineering from University of Birmingham (UK) in Dec. 2015. From May 2016 till now, he works in NUAA. His principal research interest is laser-based additive manufacturing of high performance metallic components.

Ji Ma is currently doing his master's degree in College of Materials Science and Technology, Nanjing University of Aeronautics and Astronautics (NUAA), PR China. He received the bachelor degree in Materials Processing Engineering from NUAA in Jun. 2016. His principal research interest is selective laser melting (SLM), especially majoring in the fatigue performance of titanium parts processed by SLM.

Professor Wenhua Chen is currently an Associate Professor in College of Materials Science and Technology, Nanjing University of Aeronautics and Astronautics (NUAA), PR China. He received the Master Degree of Engineering from Beihang University in Jun. 1990. From 1990 till now, he works in NUAA. His principal research interest is laser welding of metal materials, laser cladding, and laser-based additive manufacturing. Prof. Chen has authored/co-authored >30 papers in a number of internationally recognized peer-reviewed journals.

Acknowledgements

The authors gratefully acknowledge the financial support from the Innovation Fund of National Engineering and Research Center for Commercial Aircraft Manufacturing [grant number COMAC-SFGS-2016-33238]; the National Key Research and Development Program "Additive Manufacturing and Laser Manufacturing" [grant number 2016YFB1100100]; the Key Research and Development Program of Jiangsu Provincial Department of Science and Technology of China [grant number BE2016181].

References

[1] J.P. Kruth, L. Froyen, J. Van Vaerenbergh, P. Mercelis, M. Rombouts, B. Lauwers, Selective laser melting of iron-based powder, J. Mater. Process. Technol. 149 (2004) 616–622.
[2] Y. Lu, L. Ren, S. Wu, C. Yang, W. Lin, S. Xiao, Y. Yang, K. Yang, J. Lin, CoCrWCu alloy with antibacterial activity fabricated by selective laser melting: Densification, mechanical properties and microstructural analysis, Powder Technol. 325 (2018) 289–300.
[3] J. Jue, D. Gu, K. Chang, D. Dai, Microstructure evolution and mechanical properties of Al-Al_2O_3composites fabricated by selective laser melting, Powder Technol. 310 (2017) 80–91.
[4] R. Li, M. Wang, T. Yuan, B. Song, C. Chen, K. Zhou, P. Cao, Selective laser melting of a novel Sc and Zr modified Al-6.2 Mg alloy: processing, microstructure, and properties, Powder Technol. 319 (2017) 117–128.
[5] K.V. Wong, A. Hernandez, A review of additive manufacturing, ISRN Mech. Eng. 2012 (2012) 1–10.
[6] D.D. Gu, W. Meiners, K. Wissenbach, R. Poprawe, Laser additive manufacturing of metallic components: materials, processes and mechanisms, Int. Mater. Rev. 57 (2012) 133–164.
[7] L.C. Zhang, H. Attar, Selective laser melting of titanium alloys and titanium matrix composites for biomedical applications: a review, Adv. Eng. Mater. 18 (2016) 463–475.
[8] J.J. Lewandowski, M. Seifi, Metal additive manufacturing: a review of mechanical properties, Annu. Rev. Mater. Res. 46 (2016) 151–186.
[9] C.Y. Yap, C.K. Chua, Z.L. Dong, Z.H. Liu, D.Q. Zhang, L.E. Loh, S.L. Sing, Review of selective laser melting: materials and applications, Appl. Phys. Rev. 2 (2015).
[10] T. Kurzynowski, E. Chlebus, B. Kuźnicka, J. Reiner, Parameters in selective laser melting for processing metallic powders, (2012) 823914.
[11] L. Thijs, F. Verhaeghe, T. Craeghs, J. Van Humbeeck, J.P. Kruth, A study of the microstructural evolution during selective laser melting of Ti6Al4V, Acta Mater. 58 (2010) 3303–3312.
[12] B. Song, S. Dong, B. Zhang, H. Liao, C. Coddet, Effects of processing parameters on microstructure and mechanical property of selective laser melted Ti6Al4V, Mater. Des. 35 (2012) 120–125.
[13] J. Sun, Y. Yang, D. Wang, Parametric optimization of selective laser melting for forming Ti6Al4V samples by Taguchi method, Opt. Laser Technol. 49 (2013) 118–124.
[14] C. Qiu, C. Panwisawas, M. Ward, H.C. Basoalto, J.W. Brooks, M.M. Attallah, On the role of melt flow into the surface structure and porosity development during selective laser melting, Acta Mater. 96 (2015) 72–79.
[15] X. Shi, S. Ma, C. Liu, C. Chen, Q. Wu, X. Chen, J. Lu, Performance of high layer thickness in selective laser melting of Ti6Al4V, Materials 9 (2016) 1–15.
[16] L. Junfeng, W. Zhengying, Process Optimization and Microstructure Characterization of Ti6Al4V Manufactured by Selective Laser Melting, IOP Conference Series: Materials Science and Engineering. 269 (2017) 012026.
[17] J. Han, J. Yang, H. Yu, J. Yin, M. Gao, Z. Wang, X. Zeng, Microstructure and mechanical property of selective laser melted Ti6Al4V dependence on laser energy density, Rapid Prototyp. J. 23 (2017) 217–226.
[18] F. Calignano, D. Manfredi, E.P. Ambrosio, L. Iuliano, P. Fino, Influence of process parameters on surface roughness of aluminum parts produced by DMLS, Int. J. Adv. Manuf. Technol. 67 (2013) 2743–2751.
[19] K. Abd-Elghany, D.L. Bourell, Property evaluation of 304L stainless steel fabricated by selective laser melting, Rapid Prototyp. J. 18 (2012) 420–428.
[20] J.P. Choi, G.H. Shin, S. Yang, D.Y. Yang, J.S. Lee, M. Brochu, J.H. Yu, Densification and microstructural investigation of Inconel 718 parts fabricated by selective laser melting, Powder Technol. 310 (2017) 60–66.
[21] V.E. Beal, P. Erasenthiran, N. Hopkinson, P. Dickens, C.H. Ahrens, The effect of scanning strategy on laser fusion of functionally graded H13/Cu materials, Int. J. Adv. Manuf. Technol. 30 (2006) 844–852.
[22] D. Wang, Y. Yang, X. Su, Y. Chen, Study on energy input and its influences on single-track,multi-track, and multi-layer in SLM, Int. J. Adv. Manuf. Technol. 58 (2012) 1189–1199.
[23] D. Wang, Y. Yang, Z. Yi, X. Su, Research on the fabricating quality optimization of the overhanging surface in SLM process, Int. J. Adv. Manuf. Technol. 65 (2013) 1471–1484.
[24] E. Louvis, P. Fox, C.J. Sutcliffe, Selective laser melting of aluminium components, J. Mater. Process. Technol. 211 (2011) 275–284.
[25] S.L. Campanelli, N. Contuzzi, A.D. Ludovico, Manufacturing of 18 Ni Marage 300 steel samples by selective laser melting, Adv. Mater. Res. 83-86 (2009) 850–857.
[26] W. Wu, Y. Yang, D. Wang, Laser direct rapid manufacturing of functional metal part with complex structure and full density, Qiangjiguang Yu Lizishu/High Power Laser and Particle Beams, 2011.
[27] R.I.L. Guthrie, The Physical Properties of Liquid Metals, 1993.
[28] R. Eötvös, Ueber den Zusammenhang der Oberflächenspannung der Flässigkeiten mit ihrem Molecularvolumen, Ann. Phys. 263 (1886) 448–459.
[29] D. Gu, Y.C. Hagedorn, W. Meiners, G. Meng, R.J.S. Batista, K. Wissenbach, R. Poprawe, Densification behavior, microstructure evolution, and wear performance of selective laser melting processed commercially pure titanium, Acta Mater. 60 (2012) 3849–3860.
[30] R. Morgan, C.J. Sutcliffe, W. O'Neill, Density analysis of direct metal laser re-melted 316L stainless steel cubic primitives, J. Mater. Sci. 39 (2004) 1195–1205.
[31] H. Meier, C. Haberland, Experimental studies on selective laser melting of metallic parts, Mater. Werkst. 39 (2008) 665–670.
[32] M. Ma, Z. Wang, M. Gao, X. Zeng, Layer thickness dependence of performance in high-power selective laser melting of 1Cr18Ni9Ti stainless steel, J. Mater. Process. Technol. 215 (2015) 142–150.
[33] H.H. Zhu, L. Lu, J.Y.H. Fuh, Influence of binder's liquid volume fraction on direct laser sintering of metallic powder, Mater. Sci. Eng. A 371 (2004) 170–177.
[34] H. Chen, D. Gu, Effect of metallurgical defect and phase transition on geometric accuracy and wear resistance of iron-based parts fabricated by selective laser melting, J. Mater. Res. 31 (2016) 1477–1490.
[35] J. Yang, H. Yu, J. Yin, M. Gao, Z. Wang, X. Zeng, Formation and control of martensite in Ti-6Al-4V alloy produced by selective laser melting, Mater. Des. 108 (2016) 308–318.
[36] Y. Yang, Y.J. Liu, J. Chen, H.L. Wang, Z.Q. Zhang, Y.J. Lu, S.Q. Wu, J.X. Lin, Crystallographic features of α variants and β phase for Ti-6Al-4V alloy fabricated by selective laser melting, Mater. Sci. Eng. A 707 (2017) 548–558.
[37] G. Kasperovich, J. Haubrich, J. Gussone, G. Requena, Correlation between porosity and processing parameters in TiAl6V4 produced by selective laser melting, Mater. Des. 105 (2016) 160–170.
[38] L. Facchini, E. Magalini, P. Robotti, Ductility of a Ti-6Al-4V alloy produced by selective laser melting of prealloyed powders, Rapid Prototyp. 16 (2010) 450–459.
[39] S.X. Liang, M.Z. Ma, R. Jing, Y.K. Zhou, Q. Jing, R.P. Liu, Preparation of the ZrTiAlV alloy with ultra-high strength and good ductility, Mater. Sci. Eng. A 539 (2012) 42–47.
[40] R. Boyer, G. Welsch, E.W. Collings, ASM Materials Properties Handbook: Titanium Alloys, 1994.
[41] G.E. Dieter, Mechanical Metallurgy, McGrawHill, Boston, 1986 (3rd ed).